BNL-223686-2022-JAAM

Nanoscale-Femtosecond Imaging of Evanescent Surface Plasmons on Silver Film by Photon-Induced Near-Field Electron Microscopy

X. Fu, Y. Zhu

To be published in "NANO LETTERS"

March 2022

Condensed Matter Physics and Materials Science Department

Brookhaven National Laboratory

U.S. Department of Energy

USDOE Office of Science (SC), Basic Energy Sciences (BES) (SC-22)

Notice: This manuscript has been authored by employees of Brookhaven Science Associates, LLC under Contract No.DE-SC0012704 with the U.S. Department of Energy. The publisher by accepting the manuscript for publication acknowledges that the United States Government retains a non-exclusive, paid-up, irrevocable, world-wide license to publish or reproduce the published form of this manuscript, or allow others to do so, for United States Government purposes.

DISCLAIMER

This report was prepared as an account of work sponsored by an agency of the United States Government. Neither the United States Government nor any agency thereof, nor any of their employees, nor any of their contractors, subcontractors, or their employees, makes any warranty, express or implied, or assumes any legal liability or responsibility for the accuracy, completeness, or any third party's use or the results of such use of any information, apparatus, product, or process disclosed, or represents that its use would not infringe privately owned rights. Reference herein to any specific commercial product, process, or service by trade name, trademark, manufacturer, or otherwise, does not necessarily constitute or imply its endorsement, recommendation, or favoring by the United States Government or any agency thereof or its contractors or subcontractors. The views and opinions of authors expressed herein do not necessarily state or reflect those of the United States Government or any agency thereof.

Nanoscale-Femtosecond Imaging of Evanescent Surface Plasmons on Silver Film by Photon-Induced Near-Field Electron Microscopy

Authors: Xuewen Fu[1,*,†], Zepeng Sun[1,†], Shaozheng Ji[1], Fang Liu[1], Min Feng[1], Byung-Kuk Yoo[2], Yimei Zhu[3,*]

Affiliations:

[1]Ultrafast Electron Microscopy Laboratory, The MOE Key Laboratory of Weak-Light Nonlinear Photonics, School of Physics, Nankai University, Tianjin 300071, China

[2]Physical Biology Center for Ultrafast Science and Technology, Arthur Amos Noyes Laboratory of Chemical Physics, California Institute of Technology, Pasadena, CA 91125, USA

[3]Condensed Matter Physics and Materials Science Department, Brookhaven National Laboratory, Upton, New York 11973, USA

*Corresponding author. E-mail: xwfu@nankai.edu.cn; zhu@bnl.gov

†These authors contributed equally.

Keywords: Surface plasmon, PINEM, 4D electron microscopy, Energy filtered imaging, Electron energy spectrum

ABSTRACT

Surface plasmons on silver nanostructures have a wide range of tunable resonance properties in visible and near-infrared regimes, which possess a broad range of applications in nanophotonics and optoelectronics. Here we use femtosecond laser to excite surface plasmons on a silver film and trace the subsequent transient dynamics via photon-induced near-field electron microscopy (PINEM) in real time and space. We directly visualize the evanescent surface plasmons on the silver film and capture their temporal evolution using PINEM imaging on the nanometer and femtosecond scales. Polarization experiment of PINEM demonstrates that, unlike silver nanowires and nanoparticles, there is no polarization dependence of the surface plasmons and PIENM intensity on the silver film. , This is a compelling finding, suggesting a thin film platform can be easily used to identify the temporal and spatial overlaps between the pump laser and probe electron pulses in the ultrafast electron microscopy over other form of nanostructures with this technique. Our work sheds lights on the femtosecond excitation and transient behavior of the surface plasmons on sliver film and paves a universal and simple way for identifying the time zero in ultrafast electron microscopy.

INTRODUCTION

In the solid, the collective oscillations of valence electrons resemble closely the electronic plasma oscillations observed in gaseous discharges, thus the term "plasmon" is introduced to describe the quantum nature of free electron gas oscillations(*1*). If the free electron gas oscillations are driven by a light field, then their quantum representation should be a composite field consisting of the photon and the free electron gas oscillations (plasmon), or photon-plasmon polariton(*2*). Surface plasmons are collective resonant oscillations of the free electrons on the surface of metals, particularly the precious metals, for instance, silver and gold(*3-5*). These surface waves can tightly limit the electromagnetic energy(*3*). Surface plasmons combine the capabilities of photonics with the miniaturization of electronics, allowing light to be constrained to very small dimensions and its optical fields to be manipulated at the nanoscale(*6*). Such unique merits make surface plasmons a promising candidate for practical applications in many fields, such as surface-enhanced Raman spectroscopy, sensors, photovoltaic devices and quantum communication(*7-13*). Silver nanostructures are considered as one of the most important surface plasmon materials due to their wide range of tunable surface plasmon resonance properties from visible to near-infrared light regimes(*14*). The surface plasmons properties of silver nanostructures can be adjusted by changing their morphology, size and other parameters (*15-17*). For better design and use of plasmonic devices, it is important to understand the generation, propagation, and attenuation process of surface plasmons. However, all of these processes take place on the time scale of femtoseconds (fs) and the length scale of nanometers, thus it is imperative to directly characterize and capture the surface plasmons of different nanostructures of silver with high spatiotemporal resolution.

To circumvent the difficulty of tracking surface plasmons at an adequate resolution, several techniques have been devised, such as scanning near-field optical microscopy (SNOM)(*18*) and time-resolved photoemission electron microscopy (TR-PEEM)(*19*). SNOM is one of the most influential

surface plasmon imaging techniques, which is an interferometric method relying on the detection of the additional tunneling current induced by surface polaritons or the far-field scattered light due to the local surface plasmon polariton (SPP) interaction with the scanning tunneling microscopy tip. However, SNOM is not suitable to image the wave packet dynamics of the surface plasmons and its tiny microscope tip can alter the evolution of the surface plasmons(*20*). TR-PEEM is another important experimental approach to investigate the surface plasmons via photoemission electron imaging, where the plasmons greatly facilitate the multi-photon photoelectric emission process and introduce a contrast change in the PEEM image. Although TR-PEEM can image surface plasmon modes, it relies on the sample-emitted photoelectrons and the sample surface morphology. The physical processes involved in surface plasmons occur on femtosecond time scale and nanometer length scale, which makes direct visualization of evanescent surface plasmons a big experimental challenge.

4D ultrafast electron microscopy (UEM) is the most promising choice to address such a challenge due to its unique high spatiotemporal resolution imaging capability, which is achieved by integrating a fs laser with a transmission electron microscope (TEM)(*21-24*). Since the 4D UEM is based on a pump-probe approach, it can be used to perform real space imaging at the sub-nanometer scale with high temporal resolution far beyond the detector response(*25*). By introducing the strong interaction of electrons and photons into the imaging and spectroscopy methods of 4D UEM, photon-induced near-field electron microscopy (PINEM) provides the capability of directly imaging the dynamics of surface plasmons(*26-30*) on the nanometer and fs time scale. In PINEM, the inelastic electron-light interaction occurs in the presence of nanostructures, where the energy-momentum conservation condition is satisfied (*31*). As a result of this interaction, the electrons absorb or lose multiple incident photons, yielding a series of discrete peaks in the electron energy spectrum, where the peaks are separated by multiples of photon energy on both sides of the zero-loss peak (ZLP) (*26, 31-33*). When only the electrons that gained photon energy are selected by an energy filter, the fs laser pulse excited evanescent surface plasmon field can be

visualized in real space imaging of the nanostructure(*25, 26, 34, 35*). Therefore, surface plasmons can be studied by PINEM with the extremely high spatiotemporal resolution. Due to its electron penetration, non-destructive interaction, and deep subwavelength spatial and fs temporal resolution(*20*), PINEM has been used to study plasmonic interference fields at buried interfaces(*28*), plasmonic standing waves on an isolated metallic nanowire(*36*), and localized surface plasmons field of AuNPs in aqueous solution(*37*)., showing the ability to directly image the surface plasmons field distribution in real space and its temporal behavior on the fs time scale of nanostructures.

In this work, we report the study of fs laser induced evanescent surface plasmons on silver film by PINEM. We show that the fs laser induced evanescent surface plasmas on silver film can be directly imaged in real space on the fs time scales, and the strength of the surface plasmons field increases linearly with the fluence of the incident fs laser. Unlike silver nanowires or nanoparticles, we find there is no polarization dependence of the surface plasmons intensity and the PIENM intensity for the silver film, which make it an ideal platform to identify the temporal and spatial overlaps between the pump laser and probe electron pulses in 4D UEM. Our work provides a comprehensive understanding of the distribution and temporal behavior of the surface plasmons on silver film, and paves a universal and simple way for finding the time zero in 4D UEM.

RESULTS AND DISCUSSION

In our experiment, the sample is a layer of silver film (40 nm thickness) on silicon nitride membrane (see Methods and Materials) supported by a silicon frame (see the zoom-in inset on the right of **Fig. 1**), which is opaque for laser but transparent for high energy electrons. The bottom-left of **Fig.1** is a typical HAADF STEM image of the sample, showing that the silver film is quite uniform with grain size about 10 nm. The PINEEM experiments were conducted in an 4D UEM with an electron energy filter. All experiments reported here were conducted in the single-electron mode (no more than one electron per

pulse at the sample position) at a repetition of 250 kHz in order to avoid space-charge effects. The concept of the PINEM experiment is illustrated in **Fig. 1**. A fs laser pulse is split into two parts: one (green laser pulse of 517 nm) used to excite the sample and the second one (UV laser pulse of 266 nm) impinges on the cathode of the electron gun to generate photo-emitting electron pulses as the probe. After collimation and acceleration to an energy of 200 keV, the electron pulses are focused by the magnetic lens system of the TEM on the optically excited silver film. The fs time delay between the green pump laser pulses and the probe electron pulses at the sample is precisely controlled by an optical delay line.

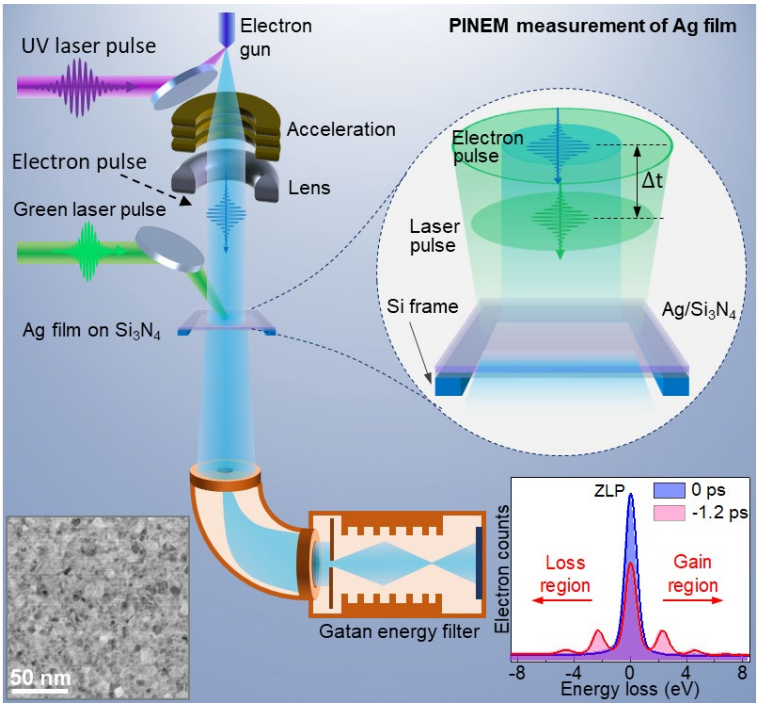

Fig. 1. PINEM measurement of sliver film. A chain of UV (266 nm) fs laser pulses is directed to the photocathode in the TEM to generate ultrafast electron pulses, which are then accelerated to 200 kV and focused to image the sample. Another chain of green laser pulses (517 nm) is focused onto the sample in the TEM to excite the surface plasmons. The electron pulses probe the sample and then enter the detector after passing through the electron energy filter. The time delay between the optical pulse and electron pulse is precisely controlled by an optical delay line. The sample is a layer of silver film (40 nm thickness, ca. 10 nm grain size) on a silicon nitride membrane supported by a silicon frame. The inset on the bottom left shows a HAADF STEM image of the sample while the one on the bottom right shows two representative PINEM spectra at t=−1.2 ps (blue curve) and 0 ps (pink curve).

Since the wave vector of the surface plasmons is always larger than that of the light in vacuum(*2, 38*), the incident light will not be able to excite the surface plasmon on a smooth metal surface due to wave vector mismatch(*2, 38, 39*). In our experiment, the surface of the silver film is rough which provides an additional horizontal momentum to the incident green laser, so that the matching condition of wave vector is satisfied and the surface plasmons can be excited(*40*). In free space, electrons and photons cannot interact with each other because of the lack of energy-momentum conservation(*30, 31*). In the high electron energy limit, conservation of energy and momentum can be reduced to the matching of the photon phase velocity and the electron group velocity(*26, 31*). For the surface plasmons, the phase velocity of light is lowered, so that the electrons and photons can be strongly coupled due to the satisfied energy-momentum conservation condition(*2, 30, 31*). Firstly, to demonstrate such coupling between the electrons and the photons, two typical fs time resolved electron energy spectra of the silver film at different delay times were recorded with 4D UEM, which is shown together at the bottom right of **Fig. 1** for comparison. One of the spectra (blue curve) was obtained when the electron pulse arrived at the sample before the fs laser pulse (t=-1.2 ps). At this point, the electrons and the photons have no interaction as they are not overlapped in time domain, and the electron spectrum only shows a ZLP. The second one (red curve) was recorded when the electron pulse and the laser pulse are timely overlapped (t=0 ps), and the electrons and the photons are strongly coupled with each other, resulting in symmetric sideband peaks separated by multiples of the photon energy on both sides of the ZLP, similar to the PINEM intensity profiles observed in metallic nanowires and nanoparticles(*26, 35, 41-43*).

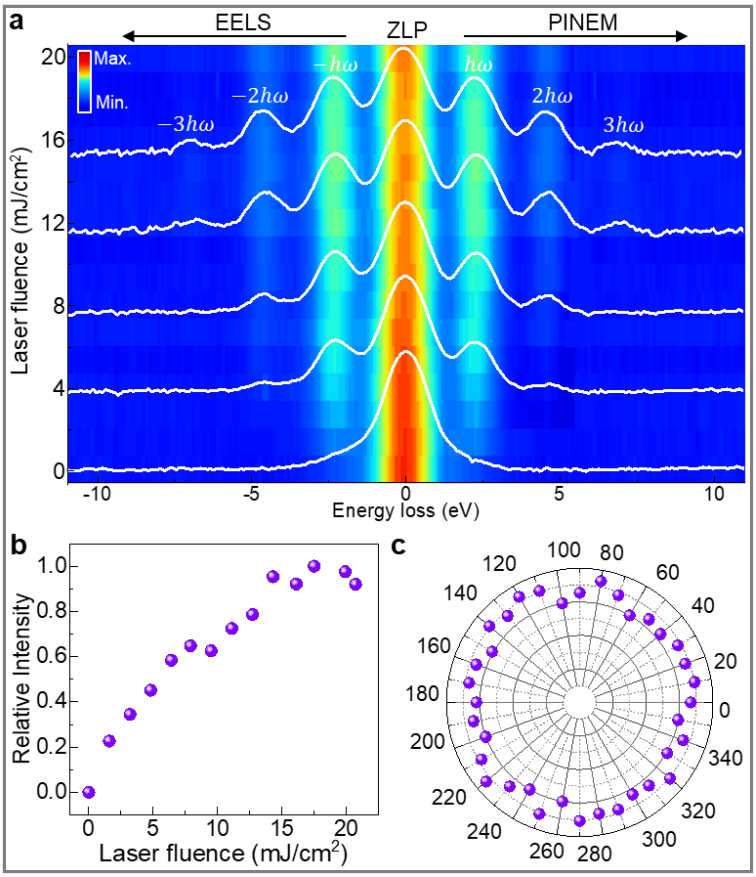

Fig. 2. Laser fluence and polarization dependence of the surface plasmons on the silver film. (**a**) Experimental measurements of electron energy loss (EELS) and gain (PINEM) as a function of the incident laser fluence. (**b**) The relative PINEM intensity as a function of the incident laser fluence. (**c**) The relative PINEM intensity evolution as a function of the polarization angle of the fs laser pulse. The radial axis of the polar coordinates represents the relative PINEM intensity, and the polarization angle is measured in degree.

Secondly, to study the laser fluence dependence of the surface plasmons, we conducted PINEM measurements on the silver film under different incident laser fluences at delay time of zero, i.e. the laser pulses and the electron pulses are fully overleaped in space and time with the maximum coupling. Note that, unlike the condition of free-electron Rabi oscillations experiment(*27*), we used the laser pulse with a smaller duration than that of the electron pulses to study the effect of laser fluence on the intensity of the surface plasmons. **Fig. 2a** shows the experimental electron energy spectroscopy intensity profiles as a function of the incident laser fluence. When the laser fluence is 0 mJ/cm^2, there is only a ZLP in the

spectrum. As the laser fluence increases, sidebands begin to appear and their intensities gradually increase. At a laser fluence of 16 mJ/cm^2 the absorption/emission of three quanta of photon energy can be clearly observed. Because the duration of the electron pulses is longer than that of the laser pulses, and the electron probe isn't focused to a tiny spot , the driving-field amplitude is not uniform during the interaction with the electron pulses(*31, 44*), and the intensity oscillation characteristic of the Bessel function dependence is suppressed in our experiment (*27, 31*). The number of sidebands is related to the strength of the interaction, indicating that the intensity of surface plasmons increases with the increase of laser fluence. By integrating the first peak of the PINEM signal of the electron energy spectra shown in **Fig. 2a**, we quantitatively studied the relationship between the laser fluence and the PINEM intensity, which is given by the square modulus of the surface plasmonic near field(*31, 32*). As shown in **Fig. 2b**, with increasing the laser fluence the PINEM intensity grows linearly first and then reaches saturation when the laser fluence arrives at ~15 mJ/cm^2, which attests that the near filed intensity of the surface plasmon increases linearly with the laser fluence before the saturation threshold. When laser fluence is higher than the threshold, the intensity of the surface plasmons saturates and there is a risk of damaging the silver film.

Besides the laser fluence dependence, we also examined the laser polarization dependence of the surface plasmons of the silver film via the electron energy spectra taken at different laser polarizations. The linearly polarized laser pulses (fluence of ~15 mJ/cm^2) was set timely overlaping with the electron pulses to maximize the electron-photon interaction in this measurement. By changing the polarization of the incident laser pulses and integrating the PINEM signal of the electron energy spectra, one can quantitatively analyze the polarization dependence of the surface plasmons on the silver film. As shown in **Fig. 2c**, there is no change in the PINEM intensity with change of the polarization angle, indicating that the intensity of the surface plasmons on the silver film has no polarization dependence. PINEM of nanostructures including silver nanowires and carbon nanotubes has been widely used to identify the temporal and spatial overlaps between pump laser pulse and probe electron pulse in the 4D UEM.

However, the surface plasmons of the nanowires and nanotubes are strongly polarization dependent and the polarization of the laser pulse should be perpendicular to the NW longitudinal axis to maximize the near-field excitation(*26*), making the use of this method limited and tedious. Unlike the nanowires, there is no polarization dependence of the PINEM for the silver film, namely, the polarization of the incident fs laser can be arbitrary, making the silver film a better platform for finding the time zero of 4D UEM.

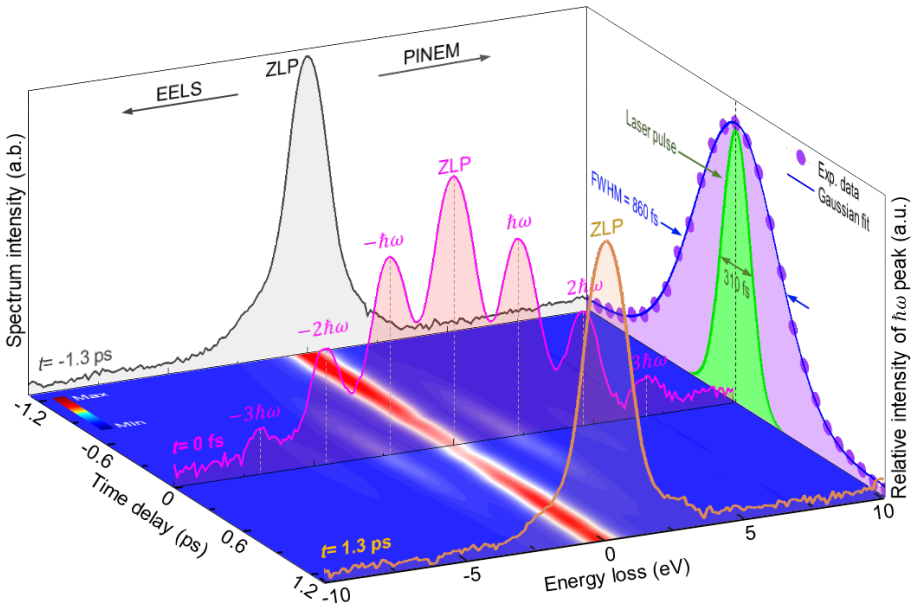

Fig. 3. Temporal evolution of the electron-energy spectra. Measured electron-energy spectra as a function of time delay between the electron pulse and the laser pulse. The right inset shows the temporal profile (purple dots) of the $\hbar\omega$ peak intensity of the electron energy spectrum with a Gaussian fit (blue curve), where the green curve shows the temporal profile of the laser pulse (duration of ~310 fs). The full width at half maximum (FWHM) of the temporal profile is ~860 fs, reflecting the duration of the electron pulse.

We further investigated the temporal evolution of the electron energy spectrum of the silver film, which can be used to determine the duration of the probe electron pulse. **Fig. 3** shows the PINEM spectrogram of photon-electron coupling between the laser pulse and the electron pulse as a function of the delay time with an excitation laser fluence of ~15 mJ/cm^2. Apparently, the electron energy spectrum consists of discrete peaks at integer multiples of $\hbar\omega$=2.4 eV (the energy of the incident photons) on both

sides of the ZLP due to the absorption/emission of photon energy through the photon-electron coupling. More intriguingly, these PINEM peaks only occur within ±0.8 ps (**Fig. 3**), indicating the transient behavior of the surface plasmons. At t=-1.3 ps, since there is no temporal overlap between the laser pulse and electron pulse and no surface plasmons is excited, there is only a zero-loss peak in the spectrum (see the gray curve in **Fig. 3**). As the temporal overlap between electron pulse and laser pulse increases, the sidebands begin to appear at t~-0.8ps, and the number and intensity of the sidebands reaches to maximum at t=0 ps (see the pink curve in **Fig. 3**). As the time delay further increases, the sidebands become weaker and finally disappear again (see the orange curve in **Fig. 3**). The temporal evolution of the $\hbar\omega$ peak intensity of the electron energy spectrum is shown on the right of **Fig. 3**, which follows a Gaussian function. Note that, the green Gaussian curve shows the temporal profile of the laser pulse (duration of ~310 fs). Through Gaussian fit and deconvolution of the laser pulse, the duration of the electron pulse at the sample position can be determined as ~860 fs.

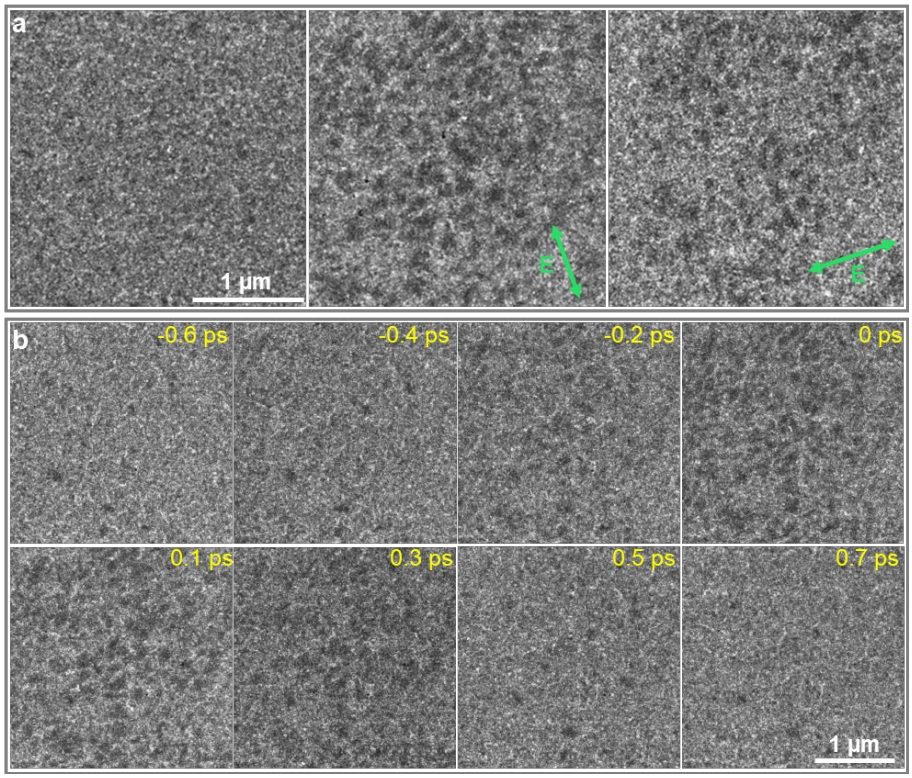

Fig. 4. Energy-filtered images of the surface plasmons in sliver film. (**a**) Typical energy-filtered images before laser excitation at t=-1.2 ps (left), energy-filtered images at t=0 ps with two different polarizations (middle and right). The green arrows indicate the direction of the laser polarization. Note the lob contrast of the grain boundaries are dominant along the direction perpendicular to the laser polarization (middle panel) and the contrast fades way when the polarization rotated 90° (right panel). (b) Energy-filtered images at different time delays, in which the polarization direction of the laser pulse is similar to that in the middle panel of (a).

Now we turn to image the surface plasmon field on the silver film using the energy-filtered imaging mode of the 4D UEM. We firstly examined the effect of laser polarization on the distribution of the surface plasmons on the silver film. By using an energy filter to select only those electrons that have absorbed $\hbar\omega$ energy to form an image, the evanescent surface plasmon field generated by the fs laser pulse became evident in the sliver film(*26, 30, 35*). To maximize the PINEM signal and the imaging contrast of the surface plasmon field, the delay time was set to t=0 ps. The left panel of **Fig. 4a** shows a bright field image obtained by energy-filtered electron pulses without laser pulse excitation, while the middle and right panels of **Fig. 4a** present similar images but after the fs laser excitation with orthogonal polarizations. As shown clearly, unlike the uniform contrast in the image before laser pump, the two images after laser pump show apparently nonuniform dark and bright contrast due the surface plasmon scattering at the grain boundaries in the silver film, where the dark particle-like contrast show the grains and the bright lob contrast indicate the grain boundaries. Notice that, although the polarization direction of the excitation laser does not affect the total PINEM intensity of the surface plasmon filed, the energy-filtered image of the surface plasmon field distribution is polarization dependent. As shown in the middle and right panels of **Fig. 4a**, the bright lob contrast of the grain boundaries are dominant along the direction perpendicular to the laser polarization direction, and the contrast diminished when the polarization direction is rotated by 90° , directly evidence that the PINEM imaging contrast is induced by the excitation laser pulses. This is because after generation the surface plasmon propagate along the polarization direction of the laser, and thus scatter at the grain boundaries perpendicular to the polarization direction. Therefore, the energy-

filtered image by the PINEM electrons can directly visualize the small gains and grain boundaries in the silver film, which are hardly to be seen in the bright field image by the electron pulses without laser pulse excitation (see left panel of **Fig. 4a**).

Since the PINEM imaging is an ultrafast - technique, by changing the time delay between the laser pulse and the electron pulse it can track the evolution of the photoexcited plasmonic wave in time, given a sufficient combined spatiotemporal resolution(*20, 26, 28*). In **Fig. 4b**, by changing the arrival time of the electron pulse at the silver film relative to the fs laser pulse, the transient evolution of the surface plasmon field was recorded in real time. The energy-filtered image at t=-0.6 ps shows almost no contrast from the plasmon field. With the temporal overlap between electron pulse and laser pulse increasing, the image contrast due to the evanescent surface plasmons field increases and reaches a maximum at t=0 ps (full overlapped) before decreasing again to almost zero at t=0.7 ps (see also the Supplementary **Movie S1**), which is in line with temporal evolution of the PINEM signal in the electron energy spectra in **Fig. 3**. Therefore, it is possible to directly capture the temporal evolution of the surface plasmon field distribution on silver films by the time-resolved real-space PINEM imaging. The ability of direct visualization of the local surface plasmon distribution and the control over its polarization and temporal behavior is of significant importance to explore the applications of silver plasmonic devices.

In conclusion, we realized the direct visualization of evanescent surface plasmons on silver film by PINEM. We found that the PINEM intensity of the surface plasmons linearly increases before reaching saturation at a laser fluence of ~15 mJ/cm^2 without polarization dependence, but the distribution of surface plasmon field depends on the laser polarization. By following PINEM image of the surface plasmon field in real time, we directly visualized the ultrafast evolution of the surface plasmon field on the silver film under fs laser excitation. Our work demonstrates the feasibility of using PINEM to study the surface plasmons in metallic films, showing its advantages of electron penetration, non-destructive interaction, fs

time resolution, and deep subwavelength spatial resolution(*20, 31, 42*). The control over the surface plasmons' polarization and temporal behavior has broad prospects in sensors, photovoltaic devices, and quantum communication etc.(*7-12*). Moreover, due to the intensity of surface plasmons is polarization independence, our work also provides a better alternative for looking for the time zero of 4D UEM.

MATERIALS AND METHODS

Preparation of Ag film

The samples studied in our experiments were prepared by electron beam evaporation of a layer of silver film (~40 nm thickness, ca. 10 nm grain size) onto a silicon nitride membrane (100 nm thickness, 300 μm × 300 μm window area) supported by a silicon frame.

PINEM measurement

The 4D UEM used in this work is based on a FEI TECNIAI G20 TEM integrated with an ultrafast amplified laser system delivering 310 fs laser pulses (wavelength of 1030 nm) at 250 kHz repetition rate to allow for both optical sample excitation and laser-driven electron pulse generation in the TEM. The UV laser pulses (wavelength of 266 nm) are generated by fourth harmonic generation and impinge on the cathode of the electron gun to generate electron pulses, while the green optical pulses (wavelength of 517 nm) are generated by second harmonic generation and are directly focused on the sample for excitation. The TEM is equipped with a Gatan imaging filter spectrometer so that we can acquire an energy-filtered image with an adjustable energy window. We employed a 3 eV wide energy window centered at the first PINEM peak of the electron spectrum for the energy-filtered images presented in this work, and the exposure time for each image is ~90 s.

SUPPLEMENTARY MATERIALS

Supplementary materials are available in the online version of the paper, including Movie S1.

REFERENCES AND NOTES

1. D. Pines, Collective Energy Losses in Solids. *Reviews of Modern Physics* **28**, 184-198 (1956).
2. Y. Fu-Zi, From plasmon to nanoplasmonics-the frontiers of modern photonics and the role of liquid crystals in tuneable nanoplasmonics. *Acta Physica Sinica* **- 64**, - 124214 (2015).
3. W. L. Barnes, A. Dereux, T. W. Ebbesen, Surface plasmon subwavelength optics. *Nature* **424**, 824-830 (2003).
4. W. A. Murray, W. L. Barnes, Plasmonic materials. *Advanced Materials* **19**, 3771-3782 (2007).
5. J. A. Schuller *et al.*, Plasmonics for extreme light concentration and manipulation. *Nat Mater* **9**, 193-204 (2010).
6. E. Ozbay, Plasmonics: merging photonics and electronics at nanoscale dimensions. *Science* **311**, 189-193 (2006).
7. H. X. Xu, E. J. Bjerneld, M. Kall, L. Borjesson, Spectroscopy of single hemoglobin molecules by surface enhanced Raman scattering. *Physical Review Letters* **83**, 4357-4360 (1999).
8. H. Xu, J. Aizpurua, M. Kall, P. Apell, Electromagnetic contributions to single-molecule sensitivity in surface-enhanced raman scattering. *Phys Rev E Stat Phys Plasmas Fluids Relat Interdiscip Topics* **62**, 4318-4324 (2000).
9. M. Moskovits, Surface-enhanced Raman spectroscopy: a brief retrospective. *Journal of Raman Spectroscopy* **36**, 485-496 (2005).
10. K. M. Mayer, J. H. Hafner, Localized surface plasmon resonance sensors. *Chem Rev* **111**, 3828-3857 (2011).
11. V. Giannini, A. I. Fernandez-Dominguez, S. C. Heck, S. A. Maier, Plasmonic Nanoantennas: Fundamentals and Their Use in Controlling the Radiative Properties of Nanoemitters. *Chemical Reviews* **111**, 3888-3912 (2011).

12. X. Guo, Y. G. Ma, Y. P. Wang, L. M. Tong, Nanowire plasmonic waveguides, circuits and devices. *Laser Photonics Rev* **7**, 855-881 (2013).
13. J. N. Anker *et al.*, Biosensing with plasmonic nanosensors. *Nature Materials*, 308-319 (2010).
14. S. Suto, K. Tsuei, E. W. Plummer, E. Burstein, Surface-plasmon energy and dispersion on Ag single crystals. *Phys Rev Lett* **63**, 2590-2593 (1989).
15. K. L. Kelly, E. Coronado, L. L. Zhao, G. C. Schatz, The Optical Properties of Metal Nanoparticles: The Influence of Size, Shape, and Dielectric Environment. *The Journal of Physical Chemistry B* **107**, 668-677 (2002).
16. D. S. Kilin, O. V. Prezhdo, Y. N. Xia, Shape-controlled synthesis of silver nanoparticles: Ab initio study of preferential surface coordination with citric acid. *Chemical Physics Letters* **458**, 113-116 (2008).
17. K. C. Lee, S. J. Lin, C. H. Lin, C. S. Tsai, Y. J. Lu, Size effect of Ag nanoparticles on surface plasmon resonance. *Surf Coat Tech* **202**, 5339-5342 (2008).
18. A. V. Zayats, I. I. Smolyaninov, A. A. Maradudin, Nano-optics of surface plasmon polaritons. *Phys Rep* **408**, 131-314 (2005).
19. H. Petek, S. Ogawa, Femtosecond time-resolved two-photon photoemission studies of electron dynamics in metals. *Progress in Surface Science* **56**, 239-310 (1997).
20. Y. Kurman *et al.*, Spatiotemporal imaging of 2D polariton wave packet dynamics using free electrons. *Science* **372**, 1181-1186 (2021).
21. V. A. Lobastov, R. Srinivasan, A. H. Zewail, Four-dimensional ultrafast electron microscopy. *Proc Natl Acad Sci U S A* **102**, 7069-7073 (2005).
22. D. Shorokhov, A. H. Zewail, 4D electron imaging: principles and perspectives. *Phys Chem Chem Phys* **10**, 2879-2893 (2008).
23. A. H. Zewail, Four-dimensional electron microscopy. *Science* **328**, 187-193 (2010).

24. J. Spencer Baskin, A. H. Zewail, Seeing in 4D with electrons: Development of ultrafast electron microscopy at Caltech. *Comptes Rendus Physique* **15**, 176-189 (2014).
25. X. Fu *et al.*, Nanoscale-femtosecond dielectric response of Mott insulators captured by two-color near-field ultrafast electron microscopy. *Nat Commun* **11**, 5770 (2020).
26. B. Barwick, D. J. Flannigan, A. H. Zewail, Photon-induced near-field electron microscopy. *Nature* **462**, 902-906 (2009).
27. A. Feist *et al.*, Quantum coherent optical phase modulation in an ultrafast transmission electron microscope. *Nature* **521**, 200-203 (2015).
28. T. T. A. Lummen *et al.*, Imaging and controlling plasmonic interference fields at buried interfaces. *Nat Commun* **7**, 13156 (2016).
29. G. M. Vanacore *et al.*, Ultrafast generation and control of an electron vortex beam via chiral plasmonic near fields. *Nat Mater* **18**, 573-579 (2019).
30. A. Yurtsever, A. H. Zewail, Direct visualization of near-fields in nanoplasmonics and nanophotonics. *Nano Lett* **12**, 3334-3338 (2012).
31. S. T. Park, M. Lin, A. H. Zewail, Photon-induced near-field electron microscopy (PINEM): theoretical and experimental. *New Journal of Physics* **12**, (2010).
32. M. T. Hassan, H. Liu, J. S. Baskin, A. H. Zewail, Photon gating in four-dimensional ultrafast electron microscopy. *Proc Natl Acad Sci U S A* **112**, 12944-12949 (2015).
33. H. Liu, J. S. Baskin, A. H. Zewail, Infrared PINEM developed by diffraction in 4D UEM. *Proc Natl Acad Sci U S A* **113**, 2041-2046 (2016).
34. O. Kfir *et al.*, Controlling free electrons with optical whispering-gallery modes. *Nature* **582**, 46-49 (2020).
35. K. Wang *et al.*, Coherent interaction between free electrons and a photonic cavity. *Nature* **582**, 50-54 (2020).

36. L. Piazza *et al.*, Simultaneous observation of the quantization and the interference pattern of a plasmonic near-field. *Nat Commun* **6**, 6407 (2015).
37. X. Fu *et al.*, Direct Visualization of Photomorphic Reaction Dynamics of Plasmonic Nanoparticles in Liquid by Four-Dimensional Electron Microscopy. *J Phys Chem Lett* **9**, 4045-4052 (2018).
38. A. A. Kolomenskii, P. D. Gershon, H. A. Schuessler, Sensitivity and detection limit of concentration and adsorption measurements by laser-induced surface-plasmon resonance. *Appl Opt* **36**, 6539-6547 (1997).
39. A. Otto, Excitation of nonradiative surface plasma waves in silver by the method of frustrated total reflection. *Zeitschrift für Physik A Hadrons and nuclei* **216**, 398-410 (1968).
40. D. N. Basov, M. M. Fogler, F. J. Garcia de Abajo, Polaritons in van der Waals materials. *Science* **354**, (2016).
41. M. T. Hassan, J. S. Baskin, B. Liao, A. H. Zewail, High-temporal-resolution electron microscopy for imaging ultrafast electron dynamics. *Nature Photonics* **11**, 425-430 (2017).
42. R. Dahan *et al.*, Resonant phase-matching between a light wave and a free-electron wavefunction. *Nature Physics* **16**, 1123-1131 (2020).
43. K. E. Echternkamp, A. Feist, S. Schäfer, C. Ropers, Ramsey-type phase control of free-electron beams. *Nature Physics* **12**, 1000-1004 (2016).
44. F. J. Garcia de Abajo, A. Asenjo-Garcia, M. Kociak, Multiphoton absorption and emission by interaction of swift electrons with evanescent light fields. *Nano Lett* **10**, 1859-1863 (2010).

Acknowledgements

This work is supported by the National Key Research and Development Program of China at grant No. 2020YFA0309300, the National Natural Science Foundation of China (NSFC) at grant No. 11974191, the Natural Science Foundation of Tianjin at grant No. 20JCZDJC00560 and 20JCJQJC00210, and the 111

Project at grant No. B07013, and the “Fundamental Research Funds for the Central Universities”，Nankai University (grant No. 91923139, 63213040 and C029211101). The work at BNL is supported by the Materials Science and Engineering Divisions, Office of Basic Energy Sciences of the U.S. Department of Energy under Contract No. DESC0012704. We acknowledge Caltech for providing the access to 4D UEM facility for this study.

Author contributions

X. F. and Y. Z. conceived the research project. X. F., and B. K. Y. did the experimental measurements. X. F. did the data analysis with input from Z. S.. X. F. and Z. S. wrote the manuscript with input from Y. Z.. All the authors contributed to the discussion and the writing of the manuscript.

Competing financial interests

The authors declare no competing financial interests.

Figure legends

Fig. 1. PINEM measurement of sliver film. A chain of UV fs laser pulses is directed to the photocathode in the TEM to generate ultrafast electron pulses, which are accelerated to 200 kV and focused to image the sample. Another chain of green laser pulses is focused onto the sample in the TEM to excite the surface plasmons. The electron pulses probe the sample and then enter the detector after passing through the electron energy filter. The time delays between the optical pulse and electron pulse is precisely controlled by an optical delay line. The sample is a layer of silver film (40 nm thickness, ca. 10 nm grain size) on a silicon nitride membrane supported by a silicon frame. The left-bottom inset shows a HAADF STEM image of the sample. The right-bottom inset shows two representative PINEM spectra at t=−1.2 ps (blue curve) and 0 ps (pink curve), respectively.

Fig. 2. Laser fluence and polarization dependence of the surface plasmons on the silver film. (a) Experimental electron energy spectrum distribution as a function of the incident laser fluence. (b) The relative PINEM intensity as a function of the incident laser fluence. (c) The relative PINEM intensity evolution as a function of the polarization angle of the fs laser pulse. The radial axis of the polar coordinates represents the relative PINEM intensity, and the unit of the polarization angle is in degree.

Fig. 3. Temporal evolution of the electron-energy spectrum. Measured electron-energy spectrum as a function of time delay between the electron pulse and the laser pulse. The right inset shows the temporal profile (purple dots) of the $\hbar\omega$ peak intensity of the electron energy spectrum with a Gaussian fit (blue curve), where the green curve shows the temporal profile of the laser pulse (duration of ~310 fs). The full width at half maximum (FWHM) of the temporal profile is ~860 fs, reflecting the duration of the electron pulse.

Fig. 4. Energy-filtered images of the surface plasmons. (a) Typical energy-filtered images without laser at t=-1.2 ps (left), energy-filtered images at t=0 ps with different polarizations (middle and right). The

green arrows indicate the direction of the laser polarization. (b) Energy-filtered images of sliver film at different time delays, in which the polarization direction of the laser pulse is similar to that in the middle panel of (a).

Figures

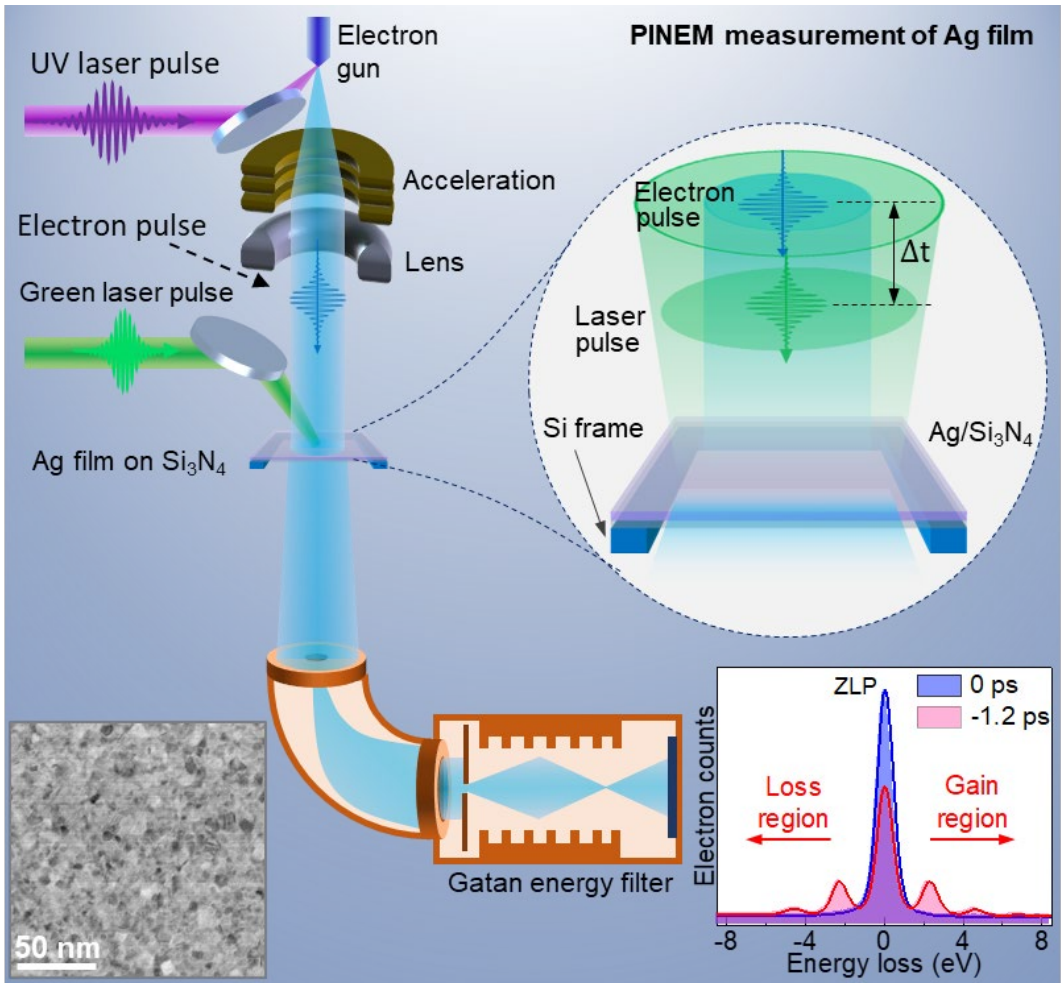

Figure 1

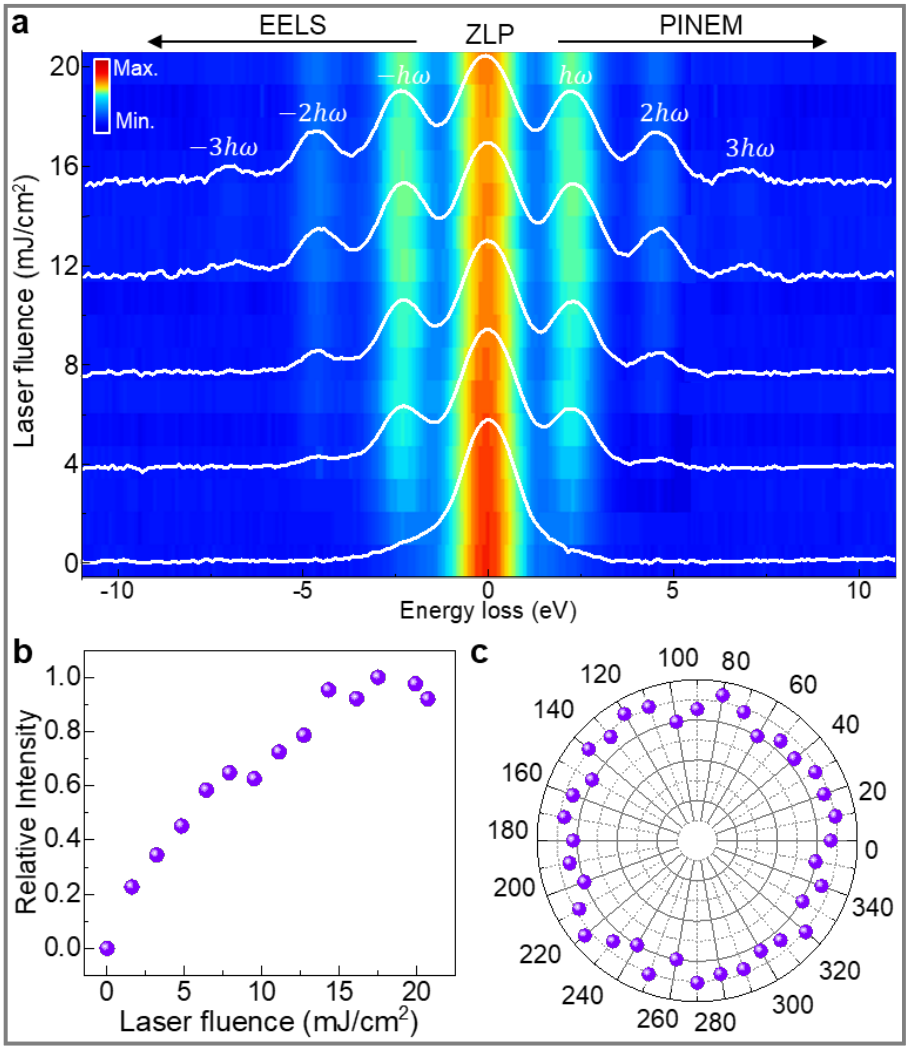
a
EELS
ZLP
PINEM
Max.
Min.
$-3\hbar\omega$
$-2\hbar\omega$
$-\hbar\omega$
$\hbar\omega$
$2\hbar\omega$
$3\hbar\omega$
Laser fluence (mJ/cm²)
Energy loss (eV)
b
Relative Intensity
Laser fluence (mJ/cm²)
c

Figure 2

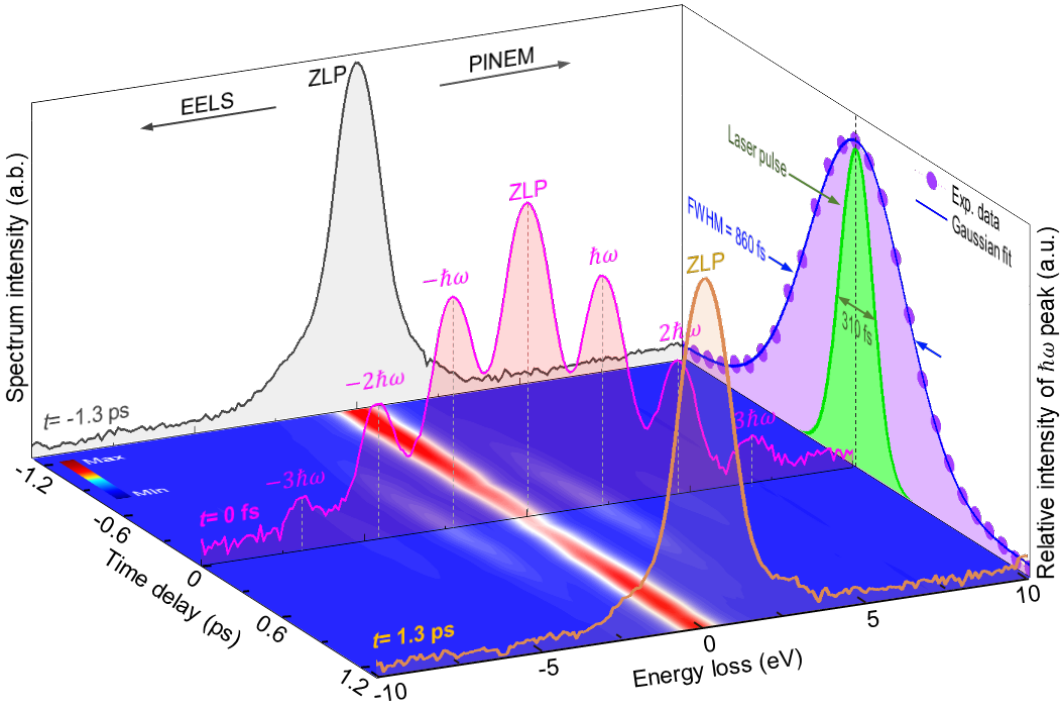
EELS
ZLP
PINEM
ZLP
$-\hbar\omega$
$\hbar\omega$
$2\hbar\omega$
ZLP
Laser pulse
FWHM = 860 fs
310 fs
Exp. data
Gaussian fit
Spectrum intensity (a.b.)
Relative intensity of $\hbar\omega$ peak (a.u.)
t= -1.3 ps
$-2\hbar\omega$
$3\hbar\omega$
$-3\hbar\omega$
Max
Min
t= 0 fs
t= 1.3 ps
-1.2
-0.6
0
0.6
1.2
Time delay (ps)
-10
-5
0
5
10
Energy loss (eV)

Figure 3

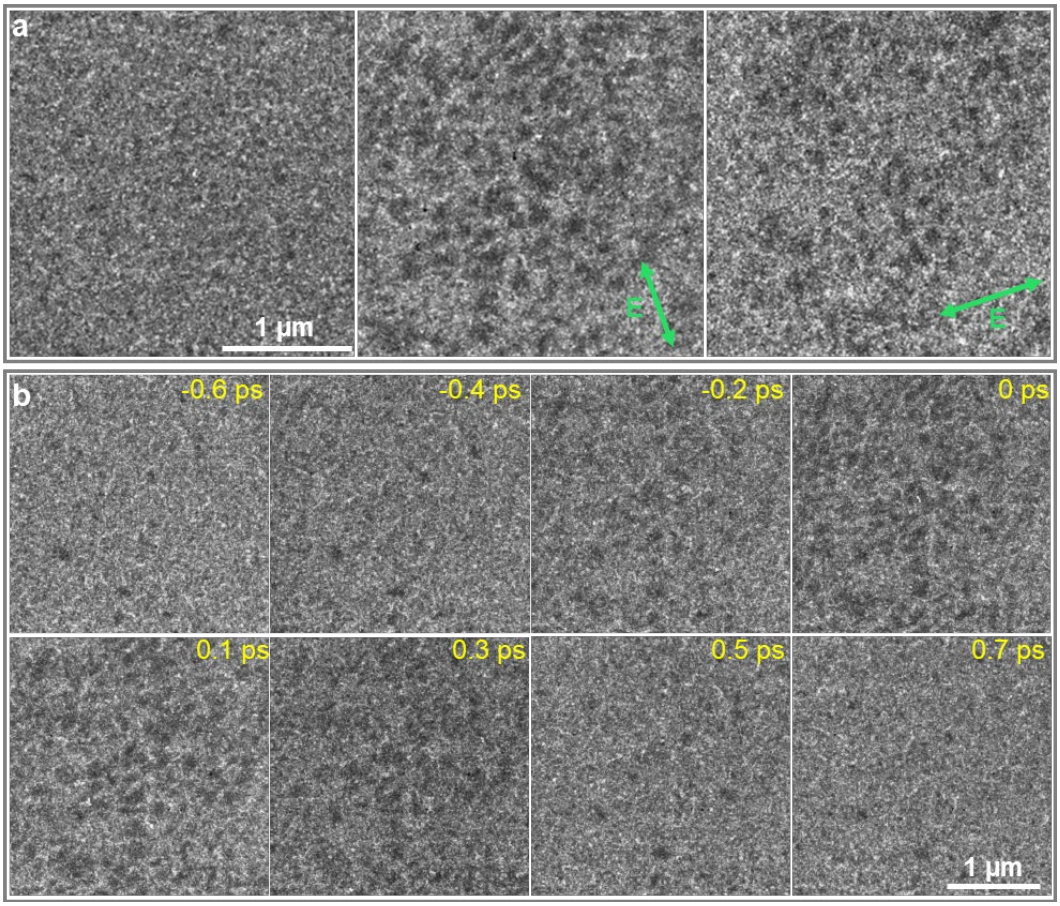

Figure 4